Biomedicine & Pharmacotherapy 145 (2022) 112380

Contents lists available at ScienceDirect

Biomedicine & Pharmacotherapy

journal homepage: www.elsevier.com/locate/biopha

Structural mechanism underlying the differential effects of ivermectin and moxidectin on the *C. elegans* glutamate-gated chloride channel GLC-2

Mark D. Kaji [a,*], Jennifer D. Noonan [a], Timothy G. Geary [a,b], Robin N. Beech [a]

[a] Institute of Parasitology, McGill University, 21111 Lakeshore Road Sainte-Anne-de-Bellevue, QC H9X 3V9, Canada
[b] School of Biological Sciences, Queen's University – Belfast, 19 Chlorine Gardens, Belfast BT9 5DL, Northern Ireland, United Kingdom

ARTICLE INFO

Keywords:
Ivermectin
Moxidectin
Glutamate-gated chloride channels
Homology model
Caenorabditis elegans
Electrophysiology

Chemical compounds studied in this article:
Ivermectin, 80:20 mixture B1a (PubChem CID: 6321424) and B1b (PubChem CID: 6321425)
Moxidectin (PubChem CID: 9832912)
Milbemycin oxime (PubChem CID: 145712259)
Selamectin PubChem CID: 9578507)

ABSTRACT

Background and purpose: Nematode glutamate-gated chloride channels (GluCls) are targets of ivermectin (IVM) and moxidectin (MOX), structurally dissimilar macrocyclic lactone (ML) anthelmintics. IVM and MOX possess different pharmacokinetics and efficacy profiles but are thought to have the same binding site, through which they allosterically activate GluCls, apart from the GLC-2 receptor, which is antagonized by IVM. Our goal was to determine GLC-2 sensitivity to MOX, investigate residues involved in antagonism of GLC-2, and to identify differences in receptor-level pharmacology between IVM and MOX.

Experimental approach: Two-electrode voltage clamp electrophysiology was used to study the pharmacology of *Caenorhabditis elegans* GLC-2 receptors heterologously expressed in *Xenopus laevis* oocytes. *In silico* homology modeling identified Cel-GLC-2 residues Met291 and Gln292 at the IVM binding site that differ from other GluCls; we mutated these residues to those found in ML-sensitive GluCls, and those of filarial nematode GLC-2.

Key results: We discovered that MOX inhibits wild-type *C. elegans* GLC-2 receptors roughly 10-fold more potently than IVM, and with greater maximal inhibition of glutamate activation (MOX = 86.9 ± 2.5%; IVM = 57.8 ± 5.9%). IVM was converted into an agonist in the Met291Gln mutant, but MOX remained an antagonist. Glutamate responses were abrogated in a Met291Leu Gln292Thr double mutant (mimicking filarial nematode GLC-2), but MOX and IVM were converted into positive allosteric modulators of glutamate at this construct.

Conclusions and implications: Our data provides new insights into differences in receptor-level pharmacology between IVM and MOX and identify residues responsible for ML antagonism of GLC-2.

1. Introduction

Macrocyclic lactones (MLs) are important broad-spectrum anthelmintics originally developed for use in veterinary medicine [1,2] and now also used for treating human filariasis and ectoparasites [3,4]. This drug family encompasses two distinct classes of molecules, avermectins and milbemycins, represented by the flagship drugs ivermectin (IVM) and moxidectin (MOX), respectively. MLs pseudoirreversibly and allosterically activate glutamate-gated chloride channels (GluCls), an invertebrate-specific receptor class of the cys-loop family of pentameric ligand-gated ion channels (pLGICs), causing hyperpolarization-induced body wall paralysis [5], inhibition of pharyngeal pumping [6], inhibition of the secretory-excretory pore [7], and persistent reduction in egg laying [8].

A crystal structure of an IVM-bound GluCl has resolved that IVM binds in the upper transmembrane (TM) region at the interface between two adjacent subunits, inserting the cyclohexene moiety towards the pore-lining (+)TM2 of the principal subunit by wedging between the (+) TM1 helix and the (-)TM3 helix of the complimentary subunit [9]. Eight nematode GluCl genes have been identified: *glc-1* (specific to *C. elegans;* does not form homomeric receptors responsive to glutamate; [10], *glc-2* [10], *glc-3* [11], *glc-4* [12,13], *glc-5* [14], *glc-6* [13], *avr-14* [15,16] and *avr-15* [17]. Of these, all but *glc-2* encode α-type IVM-sensitive GluCls; *glc-2* is the lone β-type and is antagonized by IVM [18].

Despite the atypical inhibition of homomeric GLC-2 receptors by IVM, few studies have investigated the role β-type subunits play in susceptibility to MLs. Glendinning et al. [13] showed that a triple α-GluCl null mutant clone of *C. elegans* was not paralyzed by IVM (DA1316: *avr-14*, *avr-15*, *glc-1*) and exogenous expression of GLC-2 under control of the *avr-14* promoter did not rescue IVM sensitivity,

Abbreviations: GluCl, (glutamate-gated chloride channel); IVM, (ivermectin); MOX, (moxidectin); ML, (macrocyclic lactone).

* Correspondence to: 21111 Lakeshore Road Sainte-Anne-de-Bellevue, QC H9X 3V9, Canada.
E-mail addresses: marcus.kaji@mail.mcgill.ca (M.D. Kaji), jennifer.noonan@mail.mcgill.ca (J.D. Noonan), robin.beech@mcgill.ca (R.N. Beech).

https://doi.org/10.1016/j.biopha.2021.112380
Received 7 September 2021; Received in revised form 19 October 2021; Accepted 25 October 2021
Available online 5 November 2021

suggesting that GLC-2 does not directly contribute to IVM sensitivity in worms. In contrast, El-Abdellati et al. [19] found increased *glc-2* levels among drug-resistant field isolates of the parasitic species *Cooperia oncophora*. Interestingly, it has been shown that in heteromeric *C. elegans* GLC-2/GLC-1 receptors, two GLC-2 subunits occupy the (+) position for glutamate binding in a β-α-β-α-α pattern and an α-subunit mutation in the (-)IVM binding pocket significantly affects affinity of IVM [20]. Because IVM does not activate homomeric GLC-2 receptors, this implies that the IVM binding site for agonism is restricted to (+)α-(-)α or (+)β-(-)α interfaces.

Further complicating matters is the fact that MLs encompass two structurally different classes of molecules: avermectins (i.e., IVM) and milbemycins (i.e., MOX). Resistance to both drugs has been well documented, but multiple reports indicate that MOX can retain efficacy even in the presence of IVM resistance (reviewed by [21]). Pre-exposure of COS-7 cells expressing *H. contortus* GLC-5 receptors to glutamate enhanced binding of radiolabelled IVM more than MOX [14]. This suggests a difference in affinity for the binding site, but could also represent differences in lipophilicity (for review of differences between IVM and MOX see [21]). No mechanistic explanation has been advanced for the differential pharmacology of MOX and IVM on GluCls, and the crystal structure of a MOX-bound GluCl has not been reported. We sought to determine if, like IVM, MOX antagonizes Cel-GLC-2, to identify amino acid residues that might play a role in antagonism, and to identify differences in receptor-level pharmacology between IVM and MOX.

2. Methods

2.1. Animals used: Xenopus laevis and Caenorhabditis elegans

All experiments using *X. laevis* complied with, and were approved by, McGill University and the Canadian Council on Animal Care animal protocols. All surgical procedures and animal care were performed by trained personnel as outlined in the Animal Use Protocol 2015–7758 issued by the McGill Animal Care Committee. Adult female *X. laevis* were purchased from Xenopus1 (Dexter, MI, USA).

The wild-type N2 Bristol strain of *C. elegans* was obtained from the *Caenorhabditis* Genetics Center (CGC; University of Minnesota, Minneapolis, MN, USA), funded by the US National Institutes of Health National Center for Research Resources.

2.2. Sequence analysis

All sequence analysis was performed using Geneious 9.0.5 [22]. A multiple sequence alignment (MAFFT) [23] of *C. elegans* AVR-14A (Accession #AAC25481), AVR-14B (AAC25482), AVR-15 (CAA04170), GLC-1 (NP_507090.1), GLC-2 (NP_491470), GLC-3 (CAB51708), GLC-4 (NP_495489.2), and *H. contortus* GLC-5 (AAG43233) identified two residues for site-directed mutagenesis: Met291 and Gln292 (numbering system includes signal peptide).

2.3. Phylogeny

Sequences of *glc-2* were identified from the genome data of 42 nematode species available in the WBPS13 release of the WormBase ParaSite database (International Helminth Genomes Consortium, 2019). These include *Meloidogyne hapla* (Mha), *Meloidogyne foridensis* (Mfl), *Meloidogyne incognita* (Min), *Bursaphelenchus xylophilus* (Bxy), *Globodera pallida* (Gpa), *Panagrellus redivivus* (Pre), *Enterobius vermicularis* (Eve), *Syphacia muris* (Smu), *Steinernema feltiae* (Sfe), *Steinernema carpocapsae* (Sca), *Steinernema scapterisci* (Ssc), *Pristionchus exspectatus* (Pex), *Pristionchus pacificus* (Ppa), *Camellia japonica* (Cjp), *Caenorhabditis elegans* (Cel), *Caenorhabditis sinica* (Csi), *Caenorhabditis briggsae* (Cbr), *Caenorhabditis brenneri* (Cbn), *Caenorhabditis remanei* (Cre), *Heterorhabditis bacteriophora* (Hba), *Nippostrongylus brasiliensis* (Nbr), *Haemonchus contortus* (Hco), *Necator americanus* (Nam), *Ancylostoma caninum* (Aca), *Ancylostoma ceylanicum* (Ace), *Dictyocaulus viviparus* (Dvi), *Angiostrongylus cantonensis* (Acn), *Angiostrongylus costaricensis* (Acs), *Thelazia callipaeda* (Tzc), *Dirofilaria immitis* (Dim), *Brugia malayi* (Bma), *Wuchereria bancrofti* (Wba), *Elaeophora elaphi* (Eel), *Acanthocheilonema viteae* (Avi), *Anisakis simplex* (Asi), *Ascaris lumbricoides* (Alu), *Ascaris suum* (Asu), *Toxocara canis* (Tca), *Rhabditophanes* sp. *KR3021* (Rhb), *Parastrongyloides trichosuri* (Ptr), *Strongyloides ratti* (Sra) and *Strongyloides stercoralis* (Sst). Sequences were translated and aligned using the MAFFT [23] plugin in Geneious (v 9.0.5, https://www.geneious.com/) and highly variable regions removed. These included regions within the TM3-TM4 intracellular loop, the signal peptide sequence and the C-terminal tail. A maximum likelihood phylogenetic tree was made using the PhyML plugin (v2.2.3) with default parameters and 100 bootstrap replicates [24]. Branch reliability was estimated by bootstrap resampling the dataset 100 times, and manual curation of annotations was based on the strong structural conservation of pLGIC subunits. The resulting tree's branch topology and root were compared to the Helminth Genome Consortium species tree to ensure their accuracy [25].

2.4. RNA extraction

Total RNA was isolated from two 60 mm plates of wild-type *C. elegans* washed with M9 medium (33.9 g L^{-1} Na_2HPO_4, 15 g L^{-1} KH_2PO_4, 5 g L^{-1} NH_4Cl, 2.5 g L^{-1} NaCl). Worms were crushed with a mortar and pestle and kept in liquid N_2 as they were ground into a fine powder, which was suspended in TRIzol. RNA was isolated using phenol-TRIzol purification reagents and column-purified with a Qiagen RNeasy MiniElute Cleanup Kit (Qiagen, Toronto, ON).

2.5. cDNA synthesis and cloning

First strand cDNA was synthesized using a Maxima H Minus First Strand cDNA Synthesis Kit and digested with double-stranded DNase to remove genomic DNA (Thermo Fisher Scientific, Waltham, MA). The full-length *C. elegans glc-2* coding sequence was obtained from NCBI (Accession # U14525.1) and amplified using primers flanked by 5′ *NotI* and 3′ *ApaI* restriction sites added to the ends of the primers (synthesized by Thermo Fisher Scientific). (forward primer 5′ – ATTTGCGGCCG-CATGACTACACCTAGTTCATTTTC –3′, reverse primer 5′ – ATTTGGGCCCCTAAACGAGAGACTCTGGAGTGG-3′).

PCR amplicons of 1.5 kb were gel-purified using a Zymoclean Gel DNA Recovery Kit (Cedarlane Laboratories, Ltd. Burlington, ON) for column purification and then double-digested with *NotI* and *ApaI* for ligation into the *X. laevis* oocyte expression plasmid pTD2. The pTD2 plasmid contains 5′ and 3′ UTRs of *X. laevis* β-globin designed to stabilize exogenous genes injected into oocytes and increase translation efficiency [28].

2.6. Site-directed mutagenesis

To investigate the role of residues suspected to underlie ML insensitivity in Cel-GLC-2, four different mutants were generated (Table 1). Overlapping mutagenesis primers were designed using the online Agilent QuikChange Primer Design Tool software (https://www.agilent.com/store/primerDesignProgram.jsp). Primer pairs were designed to contain base pair mismatches in the sense and antisense target site, flanked by long regions of base pairing to maximize efficiency of amplification. The high-fidelity Q5 proofreading DNA polymerase (New England Biolabs, Whitby, ON) was used to synthesize mutated copies of the entire pTD2 plasmid with the Cel-GLC-2 insert. As Q5 generates blunt-ended PCR products, amplicons were ligase-treated and *DpnI* used to eliminate methylated parental DNA. Resulting plasmids were re-grown in DH5α and sent to Genome Quebec for Sanger sequencing to verify mutagenesis.

Table 1
Sequences of primers used to create Cel-GLC-2 amino acid mutations.

	Forward primer (5′−3′)	Reverse Primer (5′−3′)
Met291Gln	GGCGTTGATTGCAGATTGCTGTGTAGTCATTGTAAGAAGCGTAG	CTACGCTTCTTACAATGACTACACAGCAATCTGCAATCAACGCC
Gln292Ser	AAGCTTGGCGTTGATTGAAGATGACATTGTAGTCATTGTAAGAAGC	GCTTCTTACAATGACTACAATGTCATCTGCAATCAACGCCAAGCTT
Met291 Gln292→ Gln291 Ser292	GGAAGCTTGGCGTTGATTGCAGATGACTGTGTAGTCATTGTAAGAAGCGTAGT	ACTACGCTTCTTACAATGACTACACAGTCATCTGCAATCAACGCCAAGCTTCC
Met291 Gln292→ Leu291 Thr292	GGAAGCTTGGCGTTGATTGCAGATGTAAGTGTAGTCATTGTAAGAAGCGTA	TACGCTTCTTACAATGACTACACTTACATCTGCAATCAACGCCAAGCTTCC

2.7. RNA synthesis

NheI-linearized pTD2 plasmid was column-purified and used as a template for *in vitro* transcription of copy RNA (cRNA) using a mMESSAGE mMACHINE T7 Transcription kit (ThermoFisher Scientific) at 37 °C for 6 h. Parental plasmid was removed by DNase treatment and the newly synthesized capped cRNA was precipitated using LiCl and resuspended in nuclease-free water at − 80 °C.

2.8. Xenopus laevis oocytes

Ovaries of *X. laevis* were surgically extracted from adult female frogs under 0.15% MS-222 tricaine methanesulphonate anesthesia (Sigma-Aldrich, Oakville, ON), neutralized to pH 7 with $NaHCO_3$. Ovary segments were cut into clumps of roughly 15 oocytes and treated with 2 mg ML^{-1} collagenase type II from *Clostridium* (Sigma-Aldrich, Oakville, ON) in Ca^{2+}-free oocyte Ringer solution (82 mM NaCl, 2 mM KCl, 1 mM $MgCl_2$, 5 mM HEPES buffer, $NaHCO_3$ to pH 7.3) to defolliculate and dissolve the tissue connecting individual oocytes. Oocytes were washed in Ringer solution to remove leftover collagenase and allowed to recover at 19 °C for 1–2 h in ND96 (96 mM NaCl, 3 mM KCl, 1 mM $MgCl_2$, 1.8 mM $CaCl_2$, 5 mM HEPES buffer, $NaHCO_3$ to pH 7.3) supplemented with pyruvate (2.5 mM) as a carbon source and penicillin (100 U ML^{-1}) and streptomycin (100 μg ML^{-1}).

2.9. Oocyte injections

To form homopentameric receptors, 25–50 ng cRNA in 50 nL was injected into the vegetal pole cytoplasm of stage V or VI oocytes using a Nanoject II (Drummond Scientific Company, Broomall, PA). Borosilicate glass injection needles were pulled from a P-1000 Flaming/Brown micropipette puller (Sutter Instrument Co, Novato, CA) and backfilled with mineral oil. To form heteromeric receptors composed of wild-type and mutant Cel-GLC-2, oocytes were injected with equal amounts of cRNA in 50 nL. Hco-GLC-5 (Accession code AAG43233; generously provided by Dr. Sean Forrester, UOIT), and Sm-GluCl-2.1 (Accession code AGV21041.1; previously cloned in our lab; [29]), served as controls for IVM-sensitive and -insensitive receptors, respectively. Water-injected oocytes acted as a negative control for membrane integrity and activity of endogenous *Xenopus* receptors. Oocytes were allowed a minimum of 24 h to synthesize and express the receptors, then were assayed daily afterwards.

2.10. Electrophysiology

Two-electrode voltage clamp (TEVC) electrophysiology was used to measure the activity of expressed ion channels. Briefly, oocytes were placed in a RC-1Z perfusion chamber (Harvard Apparatus, Saint-Laurent, QC) and pierced by two 1–5 MΩ glass microelectrodes backfilled with 3 M KCl and connected to HS-9A headstages (Axon Instruments, Foster City, CA) by Ag/AgCl wires feeding into an Axoclamp 900 A operational amplifier (Axon Instruments); oocytes were clamped at − 80 mV. The current passing headstage had a gain (h) of 1 and the voltage sensing headstage had a gain of 0.1. Wash solution (ND96 +0.1% DMSO) or drugs dissolved in ND96 was constantly gravity-perfused into the oocyte chamber and washed out with a peristatic pump. Drugs were applied until a maximal current was achieved, or after a maximum of 20 s exposure, followed by restoration of wash solution, unless specifically noted. Recordings were digitized using Digidata 1440 A (Axon Instruments). Electrophysiological recordings were analyzed using the pCLAMP11 software package, ClampFit (Molecular Devices, San Jose, CA). Currents were normalized to maximal glutamate responses from each oocyte to compare oocyte-to-oocyte.

For glutamate EC_{50} curves, oocytes were first exposed to maximal concentrations of glutamate in triplicate to establish stability of response. Then they were exposed to a range of concentrations of glutamate, with periods of saline wash in between to allow responses to return to baseline before subsequent glutamate exposure. The Leu-Thr 2X mutant glutamate EC_{50} curves were performed as above, but oocytes were first exposed to 20–30 s IVM (10 μM). To ensure that washout of IVM did not affect glutamate responses, these oocytes were exposed to 1 mM glutamate immediately after IVM (10 μM) to establish the maximal current response. After testing the range of glutamate concentrations, the final and initial 1 mM glutamate were compared and only oocytes with matching amplitudes were used for analysis.

For the Leu-Thr 2X mutant responses to 1 mM glutamate in the presence of increasing IVM concentrations, individual oocytes (n = 4 for each point on the line) were exposed to a sequence of: IVM [X] μM - glutamateA (1 mM) – IVM (10 μM) – glutamateB (1 mM) and all IVM-induced glutamateA currents were standardized as a percent of a maximal glutamateB.

For IC_{50} curves and ML inhibition, oocytes were first challenged with multiple applications of a maximal concentration of glutamate to establish stable amplitude of responses, then pre- (10 s) and co-treated with varying concentrations of IVM or MOX, up to 10 μM, with an EC_{50} concentration of glutamate to measure changes in the glutamate-induced signal. Drugs were washed out and oocyte currents allowed to return to baseline before subsequent applications. These experiments were also conducted using individual oocytes for each concentration point, standardized as a percentage of the EC_{50} glutamate response to reduce drug carryover. For mutants directly activated by IVM or MOX, each concentration of drug was compared to a 1 mM glutamate response in individual oocytes, with a minimum of 3 replicate oocytes per concentration.

To prevent carryover of MLs between oocytes, the RC-1Z chamber was removed between every recording and thoroughly washed with 70% ethanol followed by distilled water. Failure to do so yielded cross-contamination between replicates, and those oocytes were excluded from data analysis, as were oocytes unable to maintain voltage clamp and those of poor membrane integrity (current injection >1000 nA required to maintain holding potential).

Each compound was purchased from Sigma-Aldrich and dissolved in ND96 or pure DMSO and diluted in ND96 to a final 10 mM stock solution < 0.1% DMSO: L-glutamate, IVM (DMSO), MOX (DMSO), milbemycin

oxime (DMSO), selamectin (DMSO).

2.11. In silico homology modeling

Modeller 9.23 was used to generate homology models. The Hibbs & Gouaux [9] (pdb = 3RIF) Cel-GLC-1 crystal structure, in complex with glutamate and IVM, served as a template for the open channel holo conformation. For wild-type Cel-GLC-2 and each mutant receptor, 50 models were generated and the best were chosen for docking simulations based on Ramachandran plot analysis and Molpdf score (sum of all restraints) calculated by Modeller. For simplicity, results only depict a dimer of two interfacing subunits. Resulting dimers were used to prepare *in silico* ligand binding analysis of a single glutamate or ML binding site, implemented by AutoDock Vina [30]. Unless otherwise stated, molecules were instructed to bind within the volume of a 15 × 15 × 15 Å box encompassing the extracellular domain orthosteric glutamate binding site, or a 20 × 20 × 20 Å box for the allosteric ML binding site in the transmembrane domain.

Ten binding orientations were generated per root mean square from best fit using the default exhaustiveness value of 8, and the best binding poses were chosen according to predicted binding energies. Simulations with the strongest binding energies within the predicted binding pocket are depicted in Supplemental fig. All visualizations were performed using USCF Chimera [31].

2.12. Statistical analysis

Semi-log concentration-response and inhibitory curves were generated using Prism 6.0 (GraphPad Software, San Diego, CA). Prism 6.0 was used to generate graphs and for all other statistical analyses. Each oocyte represents a biological replicate, and all error bars are presented as standard error of the mean.

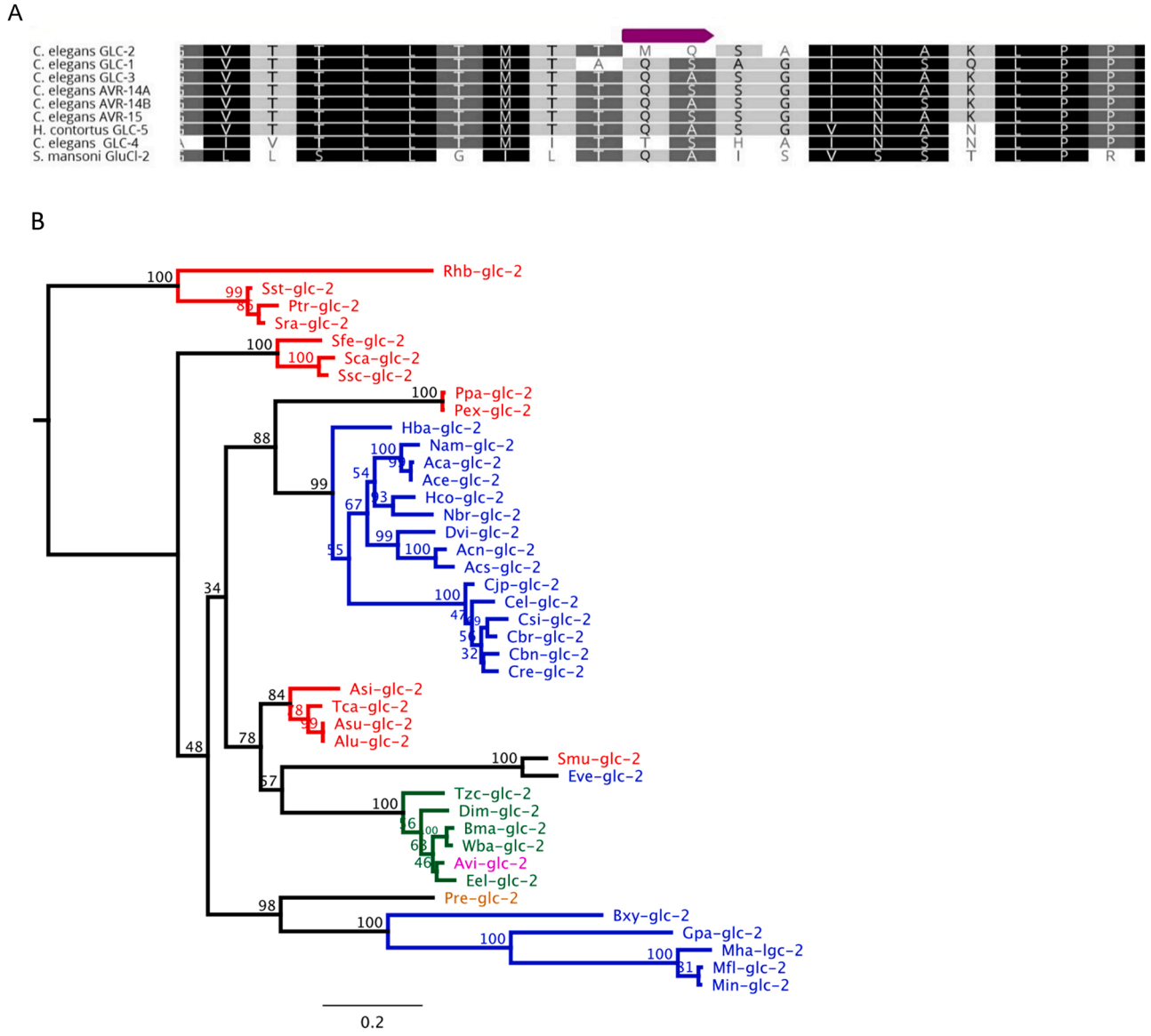

Fig. 1. (A) Sequence alignment of *C. elegans* GluCl subunits in a conserved region of the second transmembrane domain that includes the predicted IVM binding site. Sequences aligned included AVR-14A (accession # AC25481), AVR-14B (AAC25482), AVR-15 (CAA04170), GLC-1 (NP_507090.1), GLC-2 (NP_491470), GLC-3 (CAB51708), GLC-4 (NP_495489.2), *H. contortus* GLC-5 (AAG43233), and *S. mansoni* GluCl-2.1 (Accession code AGV21041.1). Presence of Met and Gln residues, indicated by purple bar, only in GLC-2 (positions 291 and 292). (B) Phylogenetic tree of *glc-2* subunits in nematodes highlighting different branches containing the conserved residues 291 and 292: blue = Met-Gln, red = Leu-Gln, green = Leu-Thr, pink = Met-Thr, orange = Val-Gln.

3. Results

3.1. Sequence analysis of Cel-GLC-2

Initial sequence alignment of *C. elegans* GluCls showed the presence of two adjacent residues, Met291-Gln292 (14′−15′ positions in literature), in TM2 of Cel-GLC-2 proximal to the predicted IVM binding site (Fig. 1A). In all α-type *C. elegans* GluCl subunits that are directly activated by IVM, these residues are Gln-Ser/Ala, respectively. We reconstructed a phylogenetic tree of GLC-2 subunits from 42 species of nematodes and identified 3 main clusters with differing motifs in this position: Met-Gln is present in clade V nematodes closely related to *C. elegans*, such as hookworms and *H. contortus*, whereas Leu-Thr is present in parasitic filarial nematodes, and Leu-Gln in *Ascaris suum, A. lumbricoides*, *Toxocara canis* and *Strongyloides stercoralis* (Fig. 1B).

3.2. Mutagenesis: glutamate responses

To investigate the role of these residues, we performed site-directed mutagenesis on Cel-GLC-2 at positions Met291 and Gln292 individually or together to generate the residues present in α-type IVM-sensitive subunits. We also changed Met-Gln→Leu-Thr to represent the residues present at these positions in filarial nematode GLC-2 (see Table 2).

Oocytes expressing Cel-GLC-2 responded to glutamate with an EC_{50} of 70.8 ± 1.1 μM (Hill coefficient = 2.8 ± 0.16). All mutants were directly activated by glutamate and with comparable but right-shifted concentration-response curves with potency in the order: wild-type > Gln292Ser > Met291Gln > Gln-Ser 2X mutant (Fig. 2A), except for the Leu-Thr 2X mutant, which produced only a minimal response to 1 mM glutamate (Fig. 2B).

Relative to maximal wild-type Cel-GLC-2 responses to glutamate (3548 ± 258 nA), only the Met291Gln mutant achieved similar channel activation (3181 ± 146 nA; Fig. 2B), whereas the Gln292Ser mutant (1974 ± 157 nA) produced maximal activation similar to the Met291Gln and Gln292Ser double mutant (2346 ± 293 nA). Unexpectedly, oocytes expressing the Leu-Thr 2X mutant had near complete attenuation of responses to glutamate, producing currents < 10 nA in response to 1 mM glutamate (Fig. 2B).

3.3. Allosteric modulation of wild-type Cel-GLC-2

To address whether MOX is an antagonist of Cel-GLC-2, we challenged oocytes expressing wild-type Cel-GLC-2 with IVM and MOX between glutamate exposures. We used the IVM-sensitive Hco-GLC-5 receptor to verify agonist activity of MOX and IVM (Figure supplement 1A,B,C), and the IVM-insensitive Sm-GluCl-2 to demonstrate specificity (Figure supplement 1D). Sm-GluCl-2 was chosen because flatworm GluCls are evolutionarily distinct from those of nematodes and are not activated by IVM [32], nor are they allosterically modulated by it. In uninjected control oocytes, we also re-applied glutamate in a similar time-course, but in the absence of ML exposure to rule out signal decay or desensitization. MLs are very lipophilic and it was possible that exposure non-specifically altered membrane fluidity, causing channels to become dysfunctional.

Neither IVM nor MOX activated Cel-GLC-2 (Fig. 3A), but both antagonized glutamate responses. To determine the extent of antagonism, we generated inhibitory concentration-response curves for IVM and MOX against an EC_{50} concentration of glutamate on Cel-GLC-2 (Fig. 3). Both drugs irreversibly inhibited glutamate-induced currents at low μM concentrations, with MOX being roughly 10-fold more potent (IVM IC_{50} = 1.28 ± 0.78 μM; Hill slope = −1.74 ± 0.76; MOX IC_{50} = 0.11 ± 1.42 μM; Hill slope = −0.65 ± 0.14). To determine whether antagonism of Cel-GLC-2 extends to other MLs, we tested milbemycin oxime and selamectin (an avermectin) and compared their responses with those of MOX and IVM (Fig. 3E). Co-treatment with any of the MLs (10 μM) produced > 50% inhibition of the glutamate response, with MOX having the greatest effect.

Table 2
Creation of the Cel-GLC-2 mutants.

Wild-type residues	Mutant products
Met291	Gln291
Gln292	Ser292
Met291 & Gln292	Gln291 & Ser292
Met291 & Gln292	Leu291 & Thr292

3.4. Leu-Thr 2X mutant

Having established ML antagonism of wild-type Cel-GLC-2, we next investigated their effects on the Met291 and Gln292 mutants. Surprisingly, the Leu-Thr 2X mutant was activated by MOX and IVM (Fig. 4). Cully et al. [10] reported that low concentrations of IVM potentiated glutamate responses in GluCls; therefore, we exposed oocytes expressing the Leu-Thr 2X mutant to a sequence of glutamate-IVM/MOX-glutamate exposures to determine whether either ML recapitulated wild-type level glutamate-induced responses. Indeed, compared to the initial glutamate response, subsequent incubation with 10 μM IVM or MOX caused a > 10-fold increase in signal amplitude after re-challenge with glutamate (maximal response roughly 950 nA). Signal enhancement was concentration-dependent for both glutamate and MLs (Fig. 4D). In the presence of 10 μM IVM, the glutamate EC_{50} was 174.3 ± 56.4 μM (Hill slope = 0.80 ± 0.32), comparable to the Gln-Ser 2X mutant in terms of glutamate potency.

3.5. α-GluCl mutant pharmacology

We next sought to determine if amino acid substitutions associated with α-type GluCl residues also generated ML activation of Cel-GLC-2. In oocytes, Gln292Ser Cel-GLC-2 was activated by IVM and MOX with the characteristic slow, irreversible hyperpolarization response seen with α-type GluCls (Fig. 5A,B). In comparison, oocytes expressing the Met291Gln mutant responded to MOX in the same way as wild-type: there was no direct activation and subsequent glutamate responses were strongly inhibited (Fig. 5 C,D). Surprisingly, IVM directly activated Met291Gln receptors (Fig. 5E). The activation (1 μM) was partially reversible only by subsequent exposure to MOX (1 μM). Furthermore, when the order of exposure was reversed, pre-treatment with 1 μM MOX for 15–20 s delayed and reduced the activation induced by 1 μM IVM (Fig. 5D; Table 3). As no GluCl has been reported to exhibit differential activation by IVM and MOX, we co-injected oocytes with cRNAs encoding the Met291Gln and Gln292Ser individual mutants in a 1:1 ratio to determine if MOX activation or inhibition was the dominant phenotype. These heteromeric receptors produced a population of channels that were directly activated by MOX (2852 ± 340 nA) with a mean current comparable to 1 mM glutamate (Fig. 5F).

We next assayed the Gln-Ser 2X mutant to determine if MOX agonist activity on the Gln292Ser single mutant was suppressed by the additional presence of the Met291Gln substitution and found these receptors to be directly activated by both IVM and MOX. To probe the potency of IVM and MOX, we compared the activation profile of a small range of concentrations (Fig. 6A). The Met291Gln mutant, followed by the Leu-Thr 2X mutant, generated the smallest IVM-induced currents, compared to Gln292Ser and the Gln-Ser 2X mutant, which produced roughly half-maximal glutamate currents in response to 1 μM MOX and IVM.

Since IVM sensitivity was the dominant phenotype of the mutants, we investigated whether co-injecting cRNAs encoding the Gln-Ser 2X mutant and wild-type Cel-GLC-2 would form receptors activated by IVM. Co-expression of these subunits in oocytes generated ML responses like the Gln-Ser 2X mutant (activated by glutamate and 1 μM IVM and MOX producing currents roughly equal to half-maximal glutamate responses;

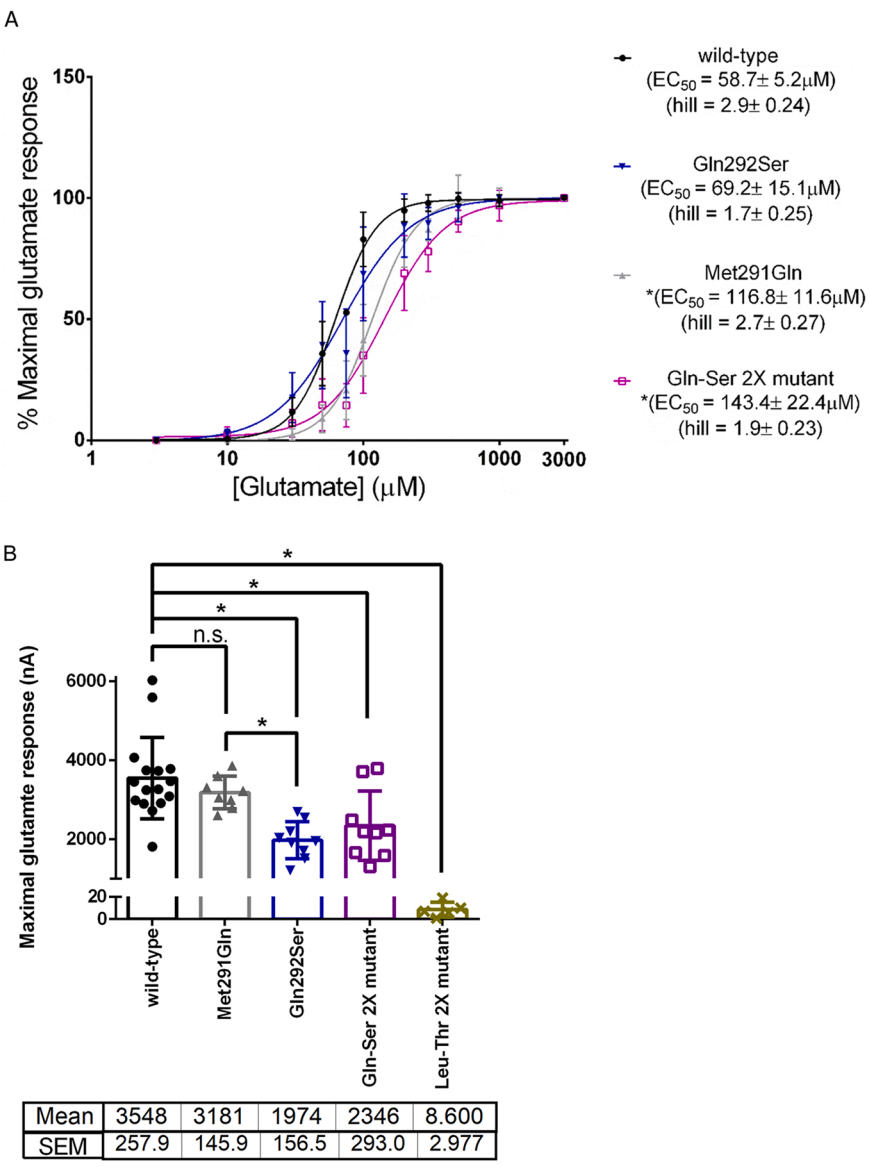

Fig. 2. (A) Concentration-response curves for glutamate activation of wild-type Cel-GLC-2 and the Met291Gln, Gln292Ser, and Met-Gln→Gln-Ser 2X mutants. The order of potency was wild-type > Gln292Ser > Met291Gln > Gln-Ser 2X mutant. In the presence of glutamate alone (1 mM), the Leu-Thr 2X mutant had < 10 nA channel activation; n > 5; only the EC_{50} of Met291Gln and the Gln-Ser 2X mutant differed significantly from wild-type, *p < 0.05 (Kruskal-Wallis test with Dunn's post-hoc) (B) Maximal currents elicited by 1 mM glutamate on wild-type and mutant Cel-GLC-2 receptors. There was no significant difference between the mean currents of Met291Gln and the Gln-Ser 2X mutant or between Gln292S and the Gln-Ser 2X mutant; n > 5; *p < 0.05 (Tukey's multiple comparison test), F = 22.91, DF = 42.

Figure supplement 2). A summary of our main electrophysiological findings can be found in Fig. 6B.

3.6. *In silico homology modeling*

We created *in silico* homology models to compare the predicted structure and ML binding site of each of the Cel-GLC-2 mutations, and the Cel-GLC-1 template as a control (Figure supplement 3A,B). Only the region proximal to the ML binding site differed between Cel-GLC-2 models. Interestingly, the best *in silico* docking simulations of IVM into a homology model of wild-type Cel-GLC-2 (−7.6 kcal mol^{-1}) failed to place the molecule between adjacent (+)TM3 and (-)TM1 subunits, but some docking simulations did predict binding within the canonical IVM binding site (−7.0 kcal mol^{-1}) (Figure supplement 3C). In contrast, no simulation placed the cyclohexene moiety of MOX proximal to (+)TM2 Gln292; rather, it presented the carbonyl of the spiroketal in this position (−8.4 kcal mol^{-1}; Figure supplement 3D), but both MLs were antagonists of this receptor in vitro.

Of the mutants in which IVM and MOX were converted into agonists, only the models of the Gln-Ser 2X mutant (IVM = −9.5 kcal mol^{-1}; MOX = −9.2 kcal mol^{-1}; Figure supplement 4A,B) and Gln292Ser (IVM = −9.2 kcal mol^{-1}; MOX = −7.9 kcal mol^{-1}; Figure supplement 4C,D) predicted ML poses within the canonical binding site with orientations and binding energies comparable to those of the GLC-1 crystal structure and our GLC-1 control simulations; however, the best Gln292Ser scoring model of MOX binding (−9.2 kcal mol^{-1}) was outside this pocket. In comparison, our models of the Leu-Thr 2X mutant placed IVM within the canonical binding site with a binding energy comparable to wild-type Cel-GLC-2 (−7.6 kcal mol^{-1}; Figure supplement 4E,F), but failed to place the cyclohexene of MOX between (+)TM3 and (-)TM1 (−8.9 kcal mol^{-1}). Interestingly, simulations of the Met291Gln mutant, where only IVM was converted into an agonist, predicted poor binding energies for IVM (+0.4 kcal mol^{-1}), whereas MOX binding (−7.8 kcal mol^{-1}) was analogous to that of wild-type Cel-GLC-2 (Figure supplement 4G,H).

4. Discussion

GLC-2 is the only β-type nematode GluCl subunit not directly activated by IVM or other MLs. However, allosteric modulation of ion channels by IVM is fairly common [33] and is a cause of neurotoxicity in ML treatment [34]. Recently, Degani-Katzav et al. [18] used a CHO expression system to show IVM antagonism of glutamate-induced currents in Cel-GLC-2. Considering these findings and the diverse activities

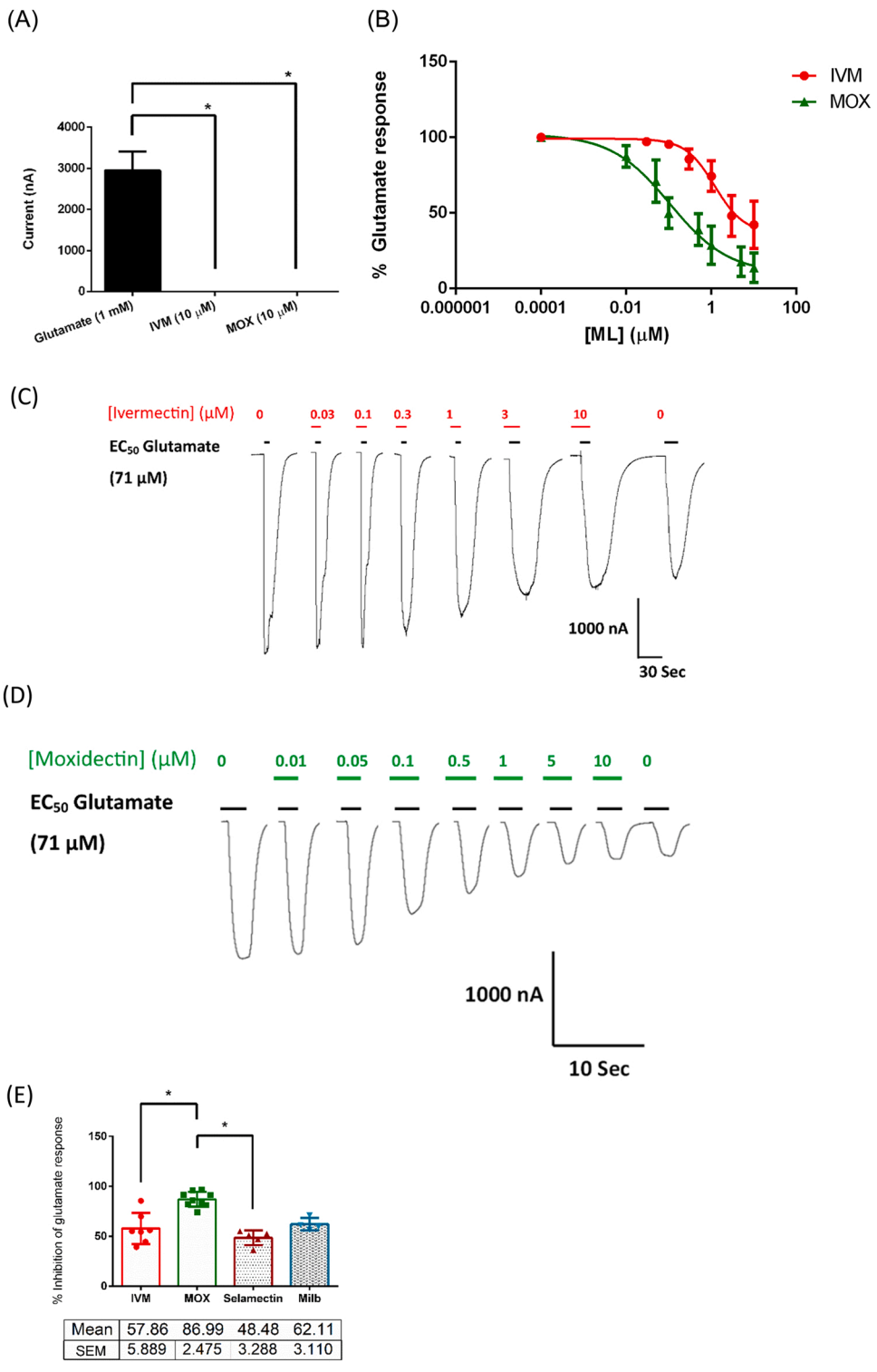

	IVM	MOX	Selamectin	Milb
Mean	57.86	86.99	48.48	62.11
SEM	5.889	2.475	3.288	3.110

Fig. 3. (A) Current response (nA) to 1 mM glutamate compared to current elicited from application of 10 μM IVM or 10 μM MOX on wild-type Cel-GLC-2 receptors; $n > 5$; *$p < 0.05$ (Kruskal-Wallis test with Dunn's post-hoc). (B) Half-maximal glutamate responses (71 μM) were inhibited by increasing concentrations of IVM or MOX. Inhibitory response curves for MOX and IVM on wild-type *C. elegans* GLC-2 in the presence of EC_{50} glutamate (IVM IC_{50} = 1.28 ± 0.78 μM; Hill slope = −1.74 ± 0.76; MOX IC_{50} = 0.11 ± 1.42 μM; Hill slope = −0.65 ± 0.14) $n \geq 5$. (C) Representative tracings of EC_{50} glutamate responses when co-applied with IVM or (D) MOX. Irreversible inhibition is indicated by the inability of drug washout to restore maximal responses to glutamate. (E) Comparison of ML (10 μM) inhibition of EC_{50} glutamate responses on Cel-GLC-2. Milb = milbemycin oxmine; $n > 4$. *$p < 0.05$ (Kruskal-Wallis test with Dunn's post-hoc).

of MLs, we initially sought to test IVM antagonism in *Xenopus* oocytes and to determine if Cel-GLC-2 was also allosterically modulated by MOX, a molecule in a different ML class.

Our data corroborate previous findings of IVM antagonism of Cel-GLC-2 and show that MOX is a more potent and efficacious antagonist than IVM. Although it is possible that these drugs possess different intrinsic affinities to bind to and inhibit Cel-GLC-2, our modeling exercises did not identify features that can readily explain differential affinity (the predicted maximal free energy of binding did not differ). A possible alternative explanation for differences in potency is that MOX accumulates to higher concentrations than IVM in the lipid microenvironment around the ML binding site and is less able to be removed by the saline wash, allowing greater binding and inhibition rates. Predicted intermolecular interactions in the IVM binding site do not feature covalent or strong ionic bonds, which together with our washout controls, suggests that these drugs very slowly exit the lipid environment of the binding site in the bilayer of the lipid membrane. Indeed, using two fluorescence-based techniques, [35] showed high accumulation of IVM in cell membranes. MOX is more lipophilic than IVM (logP: MOX=6; IVM= 4.8), which contributes to the large difference in half-life in

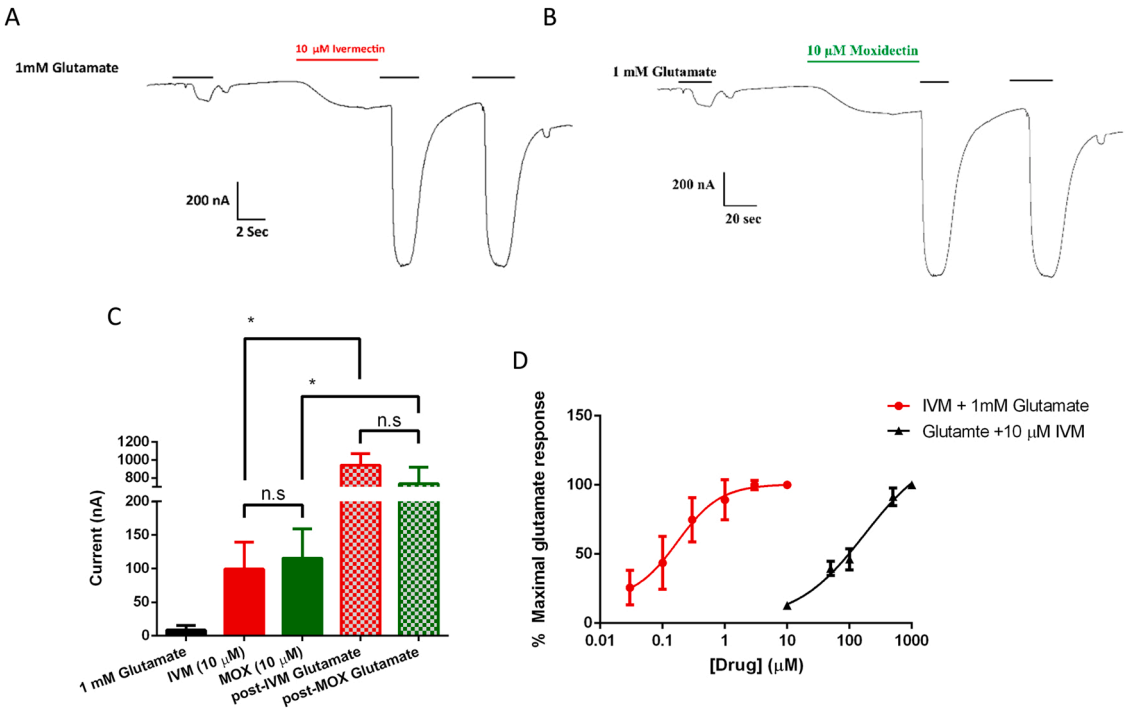

Fig. 4. (A) Representative tracing of the Leu-Thr 2X mutant showing that 10 μM IVM and (B) MOX directly activated the channel and potentiated subsequent glutamate responses. (C) MOX and IVM (10 μM) similarly activated the Leu-Thr 2X mutant, and enhanced glutamate signaling; n > 5; *p < 0.05 (Kruskal-Wallis test with Dunn's post-hoc). (D) IVM caused a concentration-dependent enhancement of 1 mM glutamate responses (red circles); EC_{99} glutamate currents produced with 6.6 μM IVM. These experiments were performed by exposing individual oocytes (n = 4 for each point on the line) to a sequence of: IVM [X] μM - glutamateA (1 mM) – IVM (10 μM) – glutamateB (1 mM) and all IVM-induced glutamateA currents were standardized as a percent of a maximal glutamateB. Glutamate responses (enhanced by an initial 10 μM IVM) were concentration-dependent (black triangles). Glutamate EC_{50} = 174.3 ± 56.4 μM (Hill slope = 0.7993 ± 0.3193); n = 4.

humans [36] and may account for greater potency at the Cel-GLC-2 receptor.

While investigating mechanisms of ML antagonism of Cel-GLC-2, we focused on two residues (Met291 and Gln292) proximal to the IVM binding site that differ in α-type IVM-sensitive *C. elegans* GluCls (relative sites described as 14′ and 15′ in literature). Homologous residues are a site of allosteric modulation by ethanol and volatile anesthetics in the $GABA_A$ receptor, and a 15′ Ser270Ile mutation is associated with altered orthosteric sensitivity, suggesting a common site of modulation [37]. In a GLC-1/GLC-2 heteropentamer, a GLC-1 Leu279Trp mutation within the (-) subunit of the IVM binding site increased potency of both glutamate and IVM, suggesting that IVM binding is allosterically coupled to glutamate binding [20]. All mutants in our study except Met291Gln had reduced responses to a saturating concentration of glutamate, supporting the role of these residues in transducing conformational changes caused by glutamate binding for channel gating. Furthermore, it has been suggested that these residues play a role in species- and subunit-specific variability in IVM responses [33].

4.1. Mutagenesis: Gln292Ser (15′) position

The crystal structure of an IVM-bound Cel-GLC-1 [9] predicts the cyclohexene hydroxyl of IVM to hydrogen bond with 15′ Ser260 of the (+)TM2 (Gln292 of Cel-GLC-2 including signal peptide). However, numerous IVM-sensitive receptors possess a small non-polar residue in this position. Furthermore, in the α1 human glycine receptor, mutating 15′ Ser to Ile did not markedly affect IVM sensitivity [38]. In comparison, in our study, Cel-GLC-2 Gln292Ser converted IVM and MOX from antagonists into agonists. Glutamine is longer than Ile and this difference in side-chain length may represent a threshold for allowing IVM and MOX to wedge deep enough between (+)TM3 (-)TM1 to permit activation, as exemplified by our *in silico* models that place IVM/MOX roughly twice as far from the 15′ position when Gln292 rather than Ser292 is present.

4.2. Mutagenesis: Met291Gln (14′) position

Whereas we anticipated Gln292Ser would influence ML activation of Cel-GLC-2, a 14′ Met is not present in any receptor known to interact with MLs, and this residue branches away from the pore but still lines the ML binding site. In a series of α1 glycine receptor mutants, Lynagh et al. [38] changed 14′ Gln to Trp and found a small improvement in IVM potency. In stark contrast, we found that substituting Met for Gln (present in α-type GluCl subunits) transformed IVM from antagonist into agonist, but MOX remained an antagonist. Permission of IVM gating in Met291Gln may be a result of changing local conformational flexibility. In the Met291Gln mutant, *in silico* analysis predicted the primary amine of the Gln to hydrogen bond with the backbone carbonyl oxygen of (+) TM1 Leu252 in the same subunit. The analogous hydrogen bond is also present in the IVM-sensitive GLC-1 model (Leu220) and may play a role in the ability of IVM to induce the conformational changes required for channel activation. Furthermore, Met can interact with aromatic residues of α-helices [39] as strong as salt bridges up to ~6 Å distances [40]. Two Cel-GLC-2 aromatic residues fit this criteria: (+)TM1 Tyr247 and (+)TM3 Trp311. Increased or altered 14′ steric hindrance may reduce the capacity of MLs to perturb local residues, preventing activation of wild-type Cel-GLC-2 receptors. Weak Met291Gln activation by IVM but not MOX is indicative of a dual role of the 14′ and 15′ positions, and suggests that, compared to MOX, IVM better fits into the binding pocket to induce activation. Many studies have shown that variations in the structure of MLs, including the absence of the disaccharide motif in MOX, play vital roles in pharmacokinetics and efficacy [34,41], but to date, no study has shown differential agonist activity between classes of ML.

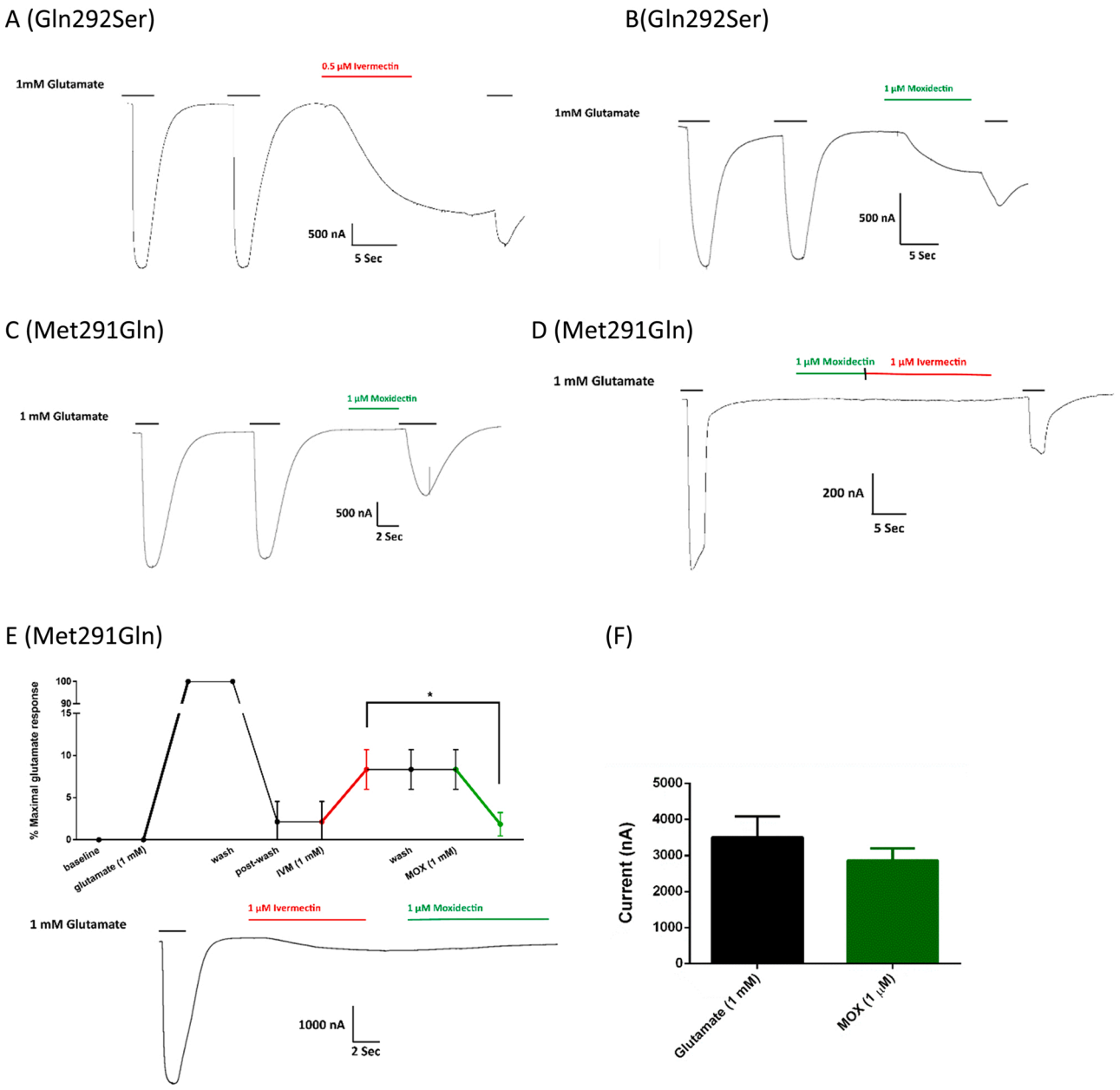

Fig. 5. (A) Representative tracing of Gln292Ser mutant activation by glutamate and IVM or (B) MOX. (C) Representative tracing showing MOX antagonism of glutamate activation of the Met291Gln mutant (D) MOX did not activate Met291Gln, but delayed and attenuated (see E) subsequent responses to IVM. (E) Tracing (bottom) and time course (top) showing activation of the Met291Gln mutant by IVM. Cessation of IVM exposure did not restore baseline, but activation was reversed by subsequent application of MOX. Initial baseline, response to glutamate, and baseline after saline wash are shown for reference; n = 6; *p < 0.05 (paired student's *t*-test). (F) Co-injecting oocytes with individual cRNAs encoding Met291Gln and Gln292Ser mutants in a 1:1 ratio produced a population of channels that were directly activated by MOX (2852 ± 340 nA [SEM]); n = 3; no significant difference of currents between 1 mM glutamate (3508 ± 580 nA) and 1 μM MOX (paired student's *t*-test).

Table 3
Met291Gln mutant responses to ivermectin and moxidectin.

	Time to IVM response after application (sec ± SEM)	*IVM response (% initial glutamate response ± SEM)*	*Amplitude of IVM response (nA ± SEM)*
No MOX pre-treatment	13.6 ± 2.1	13.7 ± 2.2	390.4 ± 125.9
15–20 s MOX pre-treatment	*34.4 ± 4.9	*4.0 ± 2.8	*26.6 ± 11.4

* p < 0.05 (paired student's *t*-tests comparing +/- MOX pre-treatment); n = 5.

4.3. Mutagenesis: Leu-Thr 2X mutant (14′ & 15′ positions)

In filarial nematodes, GLC-2 subunits have a 14′ and 15′ Leu-Thr motif. IVM is a microfilaricide that also causes prolonged sterilization of adults of some filariids, but lacks strong macrofilaricidal activity [42, 43]. Strikingly, Leu-Thr 2X mutants did not initially respond to physiologically relevant concentrations of glutamate, requiring priming by IVM or MOX to produce larger currents, similar to the phenotype of Cel-GLC-1 [44], suggesting species-specific differences in the regulation of glutamate signaling. Furthermore, the Met-Gln to Leu-Thr substitutions in Cel-GLC-2 converted IVM and MOX into weak partial agonists, comparable to their pharmacology on the Met291Gln mutant. This

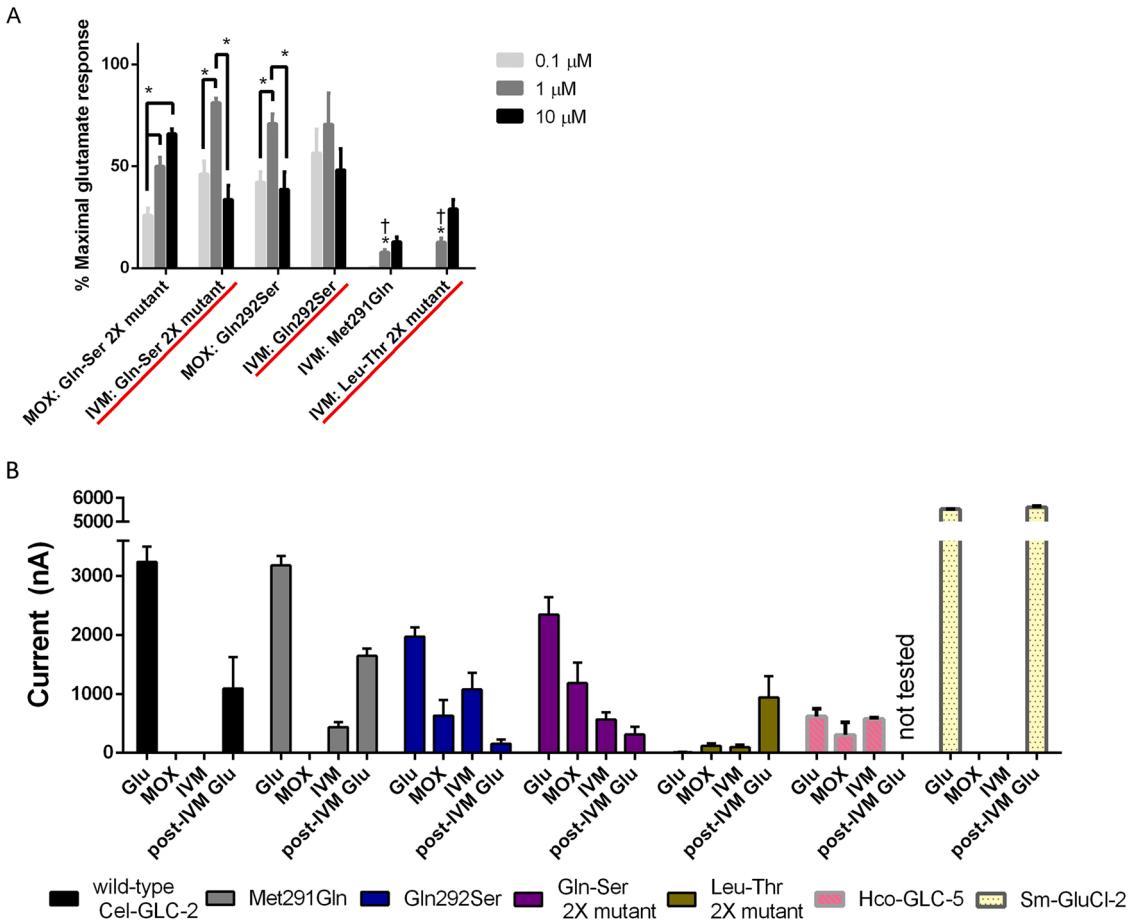

Fig. 6. (A) Agonist activity of IVM and MOX on Cel-GLC-2 mutants. The Leu-Thr 2X mutant responses were standardized to the glutamate responses enhanced by (10 μM) ML application. Individual oocytes were first exposed to 1 mM glutamate to establish a standard maximum response, then a single concentration of IVM or MOX. A minimum of 3 oocytes were used for each concentration of each ML $n \geq 3$. *$p < 0.05$ (two-way ANOVA with Bonferroni post-hoc) †0.1 μM IVM on Met291Gln and Leu-Thr 2X mutants were statistically different from the Gln292Ser, and the Gln-Ser 2X mutant responses. (B) Maximal current activation by 1 mM glutamate, 10 μM IVM, 10 μM MOX, or a re-challenge of 1 mM glutamate after IVM exposure. The Met291Gln, Gln292Ser and double mutants Gln-Ser and Leu-Thr were all activated by IVM, but only the Met291Gln mutation did not convert MOX into an agonist. *H. contortus* GLC-5 and *S. mansoni* GluCl-2 were used as controls for IVM sensitivity and insensitivity, respectively $n \geq 3$.

poses the question: do filarial nematode GLC-2 subunits fit the IVM-insensitive β-type category? Characterization of homomeric and heteromeric wild-type filarial GLC-2 will be required to determine its profile of sensitivity to avermectins and milbemycins, and whether different levels of expression and/or tissue localization can explain the different ML responses observed in these parasites.

A limitation of our study was that we did not investigate a mutant in which the 14′ and 15′ residues are Leu-Gln, which is the sequence in multiple nematode clades. Our rationale was that the Leu-Thr mutation is more relevant to the important filarial nematodes. Additionally, we separately tested each residue in the presence of glutamine in position 292 in wild-type and the Met291Gln mutant Cel-GLC-2, and the Leu in position 291 was tested in the Leu-Thr double mutant.

5. Conclusions

The pharmacodynamic significance of the Met291 and Gln292 residues for clinical *in vivo* sensitivity to IVM or MOX is unknown, but there are clear differences in Cel-GLC-2 function when these residues are changed to those found in α-type subunits or filarial β-type subunits. We show that MOX is a more potent antagonist of Cel-GLC-2 and has greater maximal inhibition than IVM, and that two adjacent residues of TM2 (Met291 and Gln292) specific to Cel-GLC-2 play a role in determining ML agonism or antagonism. More strikingly, we show evidence that IVM and MOX pharmacology rely on different residues, and that a single mutation of Cel-GLC-2 can distinguish them in terms of agonism and antagonism. These results shed light on the differential pharmacology of IVM and MOX on GluCls and suggest the importance of species-specific binding motifs for drug sensitivity and the effective control of parasitic infections.

Ethics approval statement

All experiments using *X. laevis* complied with, and were approved by, McGill University and Canadian Council on Animal Care animal protocols. All surgical procedures and animal care were performed by trained personnel as outlined in the Animal Use Protocol 2015-7758 issued by the McGill Animal Care Committee.

CRediT authorship contribution statement

Mark Kaji wrote the article, all authors contributed to editing and design. Jennifer Noonan performed the phylogenetics analysis and Mark Kaji performed all other experiments and analysis. Timothy Geary and Robin Beech supervised this project.

Declarations of interest

None.

Data availability

The data that support the findings of this study are available from the corresponding author upon reasonable request.

Acknowledgments

Funding from the NSERC-Discovery Grant program to RNB and to TGG supported this work, along with funding from the Canada Research Chairs program (TGG).

Appendix A. Supporting information

Supplementary data associated with this article can be found in the online version at doi:10.1016/j.biopha.2021.112380.

References

[1] G.W. Benz, R.A. Roncalli, S.J. Gross, Use of ivermectin in cattle, sheep, goats, and swine, in: W.C. Campbell (Ed.), Ivermectin and Abamectin, Springer, New York, 1989, pp. 215–229, https://doi.org/10.1007/978-1-4612-3626-9_15.
[2] T.J. Nolan, J.B. Lok, Macrocyclic lactones in the treatment and control of parasitism in small companion animals, Curr. Pharm. Biotechnol. 13 (2012) 1078–1094, https://doi.org/10.2174/138920112800399167.
[3] E.A. Ottesen, W.C. Campbell, Ivermectin in human medicine, J. Antimicrob. Chemother. 34 (1994) 195–203, https://doi.org/10.1093/jac/34.2.195.
[4] E.A. Ottesen, B.O. Duke, M. Karam, K. Behbehani, Strategies and tools for the control/elimination of lymphatic filariasis, Bull. World Health Organ. 75 (1997) 491–503.
[5] M.J. Turner, J.M. Schaeffer, Mode of action of ivermectin, in: W.C. Campbell (Ed.), Ivermectin and Abamectin, Springer, 1989, pp. 73–88, https://doi.org/10.1007/978-1-4612-3626-9_5.
[6] T.G. Geary, S.M. Sims, E.M. Thomas, L. Vanover, J.P. Davis, C.A. Winterrowd, R. D. Klein, N.F.H. Ho, D.P. Thompson, Haemonchus contortus: Ivermectin-induced paralysis of the pharynx, Exp. Parasitol. 77 (1993) 88–96, https://doi.org/10.1006/expr.1993.1064.
[7] Y. Moreno, J.F. Nabhan, J. Solomon, C.D. MacKenzie, T.G. Geary, Ivermectin disrupts the function of the excretory- secretory apparatus in microfilariae of Brugia malayi, Proc. Natl. Acad. Sci. USA 107 (2010) 20120–20125, https://doi.org/10.1073/pnas.1011983107.
[8] M. Walker, S.D.S. Pion, H. Fang, J. Gardon, J. Kamgno, M.G. Basáñez, M. Boussinesq, Macrofilaricidal efficacy of repeated doses of ivermectin for the treatment of river blindness, Clin. Infect. Dis. 65 (2017) 2026–2034, https://doi.org/10.1093/cid/cix616.
[9] R.E. Hibbs, E. Gouaux, Principles of activation and permeation in an anion-selective Cys-loop receptor, Nature 474 (2011) 54–60, https://doi.org/10.1038/nature10139.
[10] D.F. Cully, D.K. Vassilatis, K.K. Liu, P.S. Paress, L.H.T. Van der Ploeg, J. M. Schaeffer, J.P. Arena, Cloning of an avermectin-sensitive glutamate-gated chloride channel from Caenorhabditis elegans, Nature 371 (1994) 707–711, https://doi.org/10.1038/371707a0.
[11] L. Horoszok, V. Raymond, D.B. Sattelle, A.J. Wolstenholme, GLC-3: a novel fipronil and BIDN-sensitive, but picrotoxinin-insensitive, L-glutamate-gated chloride channel subunit from Caenorhabditis elegans, Br. J. Pharmacol. 132 (2001) 1247–1254, https://doi.org/10.1038/sj.bjp.0703937.
[12] D.F. Cully, H. Wilkinson, D.K. Vassilatis, A. Etter, J.P. Arena, Molecular biology and electrophysiology of glutamate-gated chloride channels of invertebrates, Parasitology 113 (1996) S191–S200, https://doi.org/10.1017/S0031182000077970.
[13] S.K. Glendinning, S.D. Buckingham, D.B. Sattelle, S. Wonnacott, A. J. Wolstenholme, Glutamate-gated chloride channels of Haemonchus contortus restore drug sensitivity to ivermectin resistant Caenorhabditis elegans, PLoS One 6 (2011), e22390, https://doi.org/10.1371/journal.pone.0022390.
[14] S.G. Forrester, R.K. Prichard, R.N. Beech, A glutamate-gated chloride channel subunit from Haemonchus contortus: expression in a mammalian cell line, ligand binding, and modulation of anthelmintic binding by glutamate, Biochem. Pharmacol. 63 (2002) 1061–1068, https://doi.org/10.1016/S0006-2952(02)00852-3.
[15] D.L. Laughton, G.G. Lunt, A.J. Wolstenholme, Alternative splicing of a Caenorhabditis elegans gene produces two novel inhibitory amino acid receptor subunits with identical ligand binding domains but different ion channels, Gene 201 (1997) 119–125, https://doi.org/10.1016/S0378-1119(97)00436-8.
[16] J.A. Dent, M.M. Smith, D.K. Vassilatis, L. Avery, The genetics of ivermectin resistance in Caenorhabditis elegans, Proc. Natl. Acad. Sci. USA 97 (2000) 2674–2679, https://doi.org/10.1073/pnas.97.6.2674.
[17] J.A. Dent, M. Davins, L. Avery, avr-15 encodes a chloride channel subunit that mediates inhibitory glutamatergic neurotransmission and ivermectin sensitivity in Caenorhabditis elegans, EMBO J. 16 (1997) 5867–5879, https://doi.org/10.1093/emboj/16.19.5867.
[18] N. Degani-Katzav, M. Klein, M. Har-Even, R. Gortler, R. Tobi, Y. Paas, Trapping of ivermectin by a pentameric ligand-gated ion channel upon open-to-closed isomerization, Sci. Rep. 7 (2017) 1–18, https://doi.org/10.1038/srep42481.
[19] A. El-Abdellati, J. De Graef, A. Van Zeveren, A. Donnan, P. Skuce, T. Walsh, A. Wolstenholme, A. Tait, J. Vercruysse, E. Claerebout, P. Geldhof, Altered avr-14B gene transcription patterns in ivermectin-resistant isolates of the cattle parasites, Cooperia oncophora and Ostertagia ostertagi, Int. J. Parasitol. 41 (2011) 951–957, https://doi.org/10.1016/j.ijpara.2011.04.003.
[20] N. Degani-Katzav, R. Gortler, L. Gorodetzki, Y. Paas, Subunit stoichiometry and arrangement in a heteromeric glutamate-gated chloride channel, Proc. Natl. Acad. Sci. USA 113 (2016) E644–E653, https://doi.org/10.1073/pnas.1423753113.
[21] R.K. Prichard, T.G. Geary, Perspectives on the utility of moxidectin for the control of parasitic nematodes in the face of developing anthelmintic resistance, Int. J. Parasitol. Drugs Drug Resist. 10 (2019) 69–83, https://doi.org/10.1016/j.ijpddr.2019.06.002.
[22] M. Kearse, R. Moir, A. Wilson, S. Stones-Havas, M. Cheung, S. Sturrock, S. Buxton, A. Cooper, S. Markowitz, C. Duran, T. Thierer, B. Ashton, P. Meintjes, A. Drummond, Geneious Basic: an integrated and extendable desktop software platform for the organization and analysis of sequence data, Bioinformatics 28 (2012) 1647–1649, https://doi.org/10.1093/bioinformatics/bts199.
[23] K. Katoh, D.M. Standley, MAFFT multiple sequence alignment software version 7: improvements in performance and usability, Mol. Biol. Evol. 30 (2013) 772–780, https://doi.org/10.1093/molbev/mst010.
[24] S. Guindon, J.F. Dufayard, V. Lefort, M. Anisimova, W. Hordijk, O. Gascuel, New algorithms and methods to estimate maximum-likelihood phylogenies: assessing the performance of PhyML 3.0, Syst. Biol. 59 (2010) 307–321, https://doi.org/10.1093/sysbio/syq010.
[25] International Helminth Genomes Consortium, Comparative genomics of the major parasitic worms, Nat. Genet. 51 (2019) 163–174, https://dx.doi.org/10.1038%2Fs41588-018-0262-1.
[28] T.B. Duguet, C.L. Charvet, S.G. Forrester, C.M. Wever, J.A. Dent, C. Neveu, R. N. Beech, Recent duplication and functional divergence in parasitic nematode levamisole-sensitive acetylcholine receptors, PLoS Negl. Trop. Dis. 10 (2016), e0004826, https://doi.org/10.1371/journal.pntd.0004826.
[29] V. Dufour, R.N. Beech, C. Wever, J.A. Dent, T.G. Geary, Molecular cloning and characterization of novel glutamate-gated chloride channel subunits from Schistosoma mansoni, PLoS Pathog. 9 (2013), e1003586, https://doi.org/10.1371/journal.ppat.1003586.
[30] O. Trott, A.J. Olson, AutoDock Vina: improving the speed and accuracy of docking with a new scoring function, efficient optimization, and multithreading, J. Comput. Chem. 31 (2010) 455–461, https://doi.org/10.1002/jcc.21334.
[31] E.F. Pettersen, T.D. Goddard, C.C. Huang, G.S. Couch, D.M. Greenblatt, E.C. Meng, T.E. Ferrin, UCSF Chimera—a visualization system for exploratory research and analysis, J. Comput. Chem. 25 (2004) 1605–1612, https://doi.org/10.1002/jcc.20084.
[32] T. Lynagh, R.N. Beech, M.J. Lalande, K. Keller, B.A. Cromer, A.J. Wolstenholme, B. Laube, Molecular basis for convergent evolution of glutamate recognition by pentameric ligand-gated ion channels, Sci. Rep. 5 (2015) 8558, https://doi.org/10.1038/srep08558.
[33] T. Lynagh, J.W. Lynch, Ivermectin binding sites in human and invertebrate Cys-loop receptors, Trends Pharmacol. Sci. 33 (2012) 432–441, https://doi.org/10.1016/j.tips.2012.05.002.
[34] C. Ménez, J.F. Sutra, R. Prichard, A. Lespine, Relative neurotoxicity of ivermectin and moxidectin in mdr1ab (-/-) mice and effects on mammalian GABA(A) channel activity, PLoS Negl. Trop. Dis. 6 (2012), e1883, https://doi.org/10.1371/journal.pntd.0001883.
[35] M. Atif, J.J. Smith, A. Estrada-Mondragon, X. Xiao, A.A. Salim, R.J. Capon, J. W. Lynch, A. Keramidas, GluClR-mediated inhibitory postsynaptic currents reveal targets for ivermectin and potential mechanisms of ivermectin resistance, PLoS Pathog. 15 (2019), e1007570, https://doi.org/10.1371/journal.ppat.1007570.
[36] P. Milton, J.I.D. Hamley, M. Walker, M.G. Basáñez, Moxidectin: an oral treatment for human onchocerciasis, Expert Rev. Anti-Infect. Ther. 18 (2020) 1067–1081, https://doi.org/10.1080/14787210.2020.1792772.
[37] S.J. Mihic, Q. Ye, M.J. Wick, V.V. Koltchine, M.D. Krasowski, S.E. Finn, M. P. Mascia, C.F. Valenzuela, K.K. Hanson, E.P. Greenblatt, R.A. Harris, N. L. Harrison, Sites of alcohol and volatile anaesthetic action on GABA A and glycine receptors, Nature 389 (1997) 385–389, https://doi.org/10.1038/38738.
[38] T. Lynagh, T.I. Webb, C.L. Dixon, B.A. Cromers, J.W. Lynch, Molecular determinants of ivermectin sensitivity at the glycine receptor chloride channel, J. Biol. Chem. 286 (2011) 43913–43924, https://doi.org/10.1074/jbc.M111.262634.
[39] A.R. Viguera, L. Serrano, Side-chain interactions between sulfur-containing amino acids and phenyalanine in alpha-helixes, Biochemistry 34 (1995) 8771–8779, https://doi.org/10.1021/bi00027a028.
[40] C.C. Valley, A. Cembran, J.D. Perlmutter, A.K. Lewis, N.P. Labello, J. Gao, J. N. Sachs, The methionine-aromatic motif plays a unique role in stabilizing protein structure, J. Biol. Chem. 287 (2012) 34979–34991, https://doi.org/10.1074/jbc.M112.374504.
[41] B. Michael, P.T. Meinke, W. Shoop, Comparison of ivermectin, doramectin, selamectin, and eleven intermediates in a nematode larval development assay, J. Parasitol. 87 (2001) 692–696, https://doi.org/10.1645/0022-3395(2001)087[0692:COIDSA]2.0.CO;2.

[42] G. Dreyer, J. Noroes, F. Amaral, A. Nen, Z. Medeiros, A. Coutinho, D. Addiss, Direct assessment of the adulticidal efficacy of a single dose of ivermectin in bancroftian filariasis, Trans. R. Soc. Trop. Med. Hyg. 89 (1995) 441–443, https://doi.org/10.1016/0035-9203(95)90049-7.

[43] J.W. McCall, J. Guerrero, R.E. Roberts, N. Supakorndej, A.E. Mansour, M. T. Dzimianski, Further evidence of clinical prophylactic, retro-active (reach-back) and adulticidal activity of monthly administrations of ivermectin (Heartgard PlusTM) in dogs experimentally infected with heartworms, in: R.L. Seward (Ed.), Recent Advances in Heartworm Disease, Symposium '01, American Heartworm Society, Batavia, Illinois, 2001, pp. 189–200.

[44] A. Etter, D.F. Cully, J.M. Schaeffer, K.K. Liu, J.P. Arena, An amino acid substitution in the pore region of a glutamate-gated chloride channel enables the coupling of ligand binding to channel gating, J. Biol. Chem. 271 (1996) 16035–16039, https://doi.org/10.1074/jbc.271.27.16035.